


Structural Connectivity-Based Topography of the Human Globus Pallidus: Implications for Therapeutic Targeting in Movement Disorders

Alberto Cacciola, MD,^{1*}  Demetrio Milardi, MD, PhD,^{1,2} Salvatore Bertino, MD,¹ Gianpaolo Antonio Basile, MD,¹ Alessandro Calamuneri, PhD,² Gaetana Chillemi, PhD,² Giuseppina Rizzo, MD,¹ Giuseppe Anastasi, MD,¹ and Angelo Quartarone, MD^{1*}

¹Department of Biomedical, Dental Sciences and Morphological and Functional Images, University of Messina, Messina, Italy

²IRCCS Centro Neurolesi "Bonino Pulejo", Messina, Italy

ABSTRACT: Background: Understanding the topographical organization of the cortico-basal ganglia circuitry is of pivotal importance because of the spreading of techniques such as DBS and, more recently, MR-guided focused ultrasound for the treatment of movement disorders. A growing body of evidence has described both direct cortico- and dento-pallidal connections, although the topographical organization in vivo of these pathways in the human brain has never been reported.

Objective: To investigate the topographical organization of cortico- and dento-pallidal pathways by means of diffusion MRI tractography and connectivity based parcellation.

Methods: High-quality data from 100 healthy subjects from the Human Connectome Project repository were utilized. Constrained spherical deconvolution-based tractography was used to reconstruct structural cortico- and dento-pallidal connectivity. Connectivity-based parcellation was performed with a hypothesis-driven approach at three different levels: functional regions (limbic, associative, sensorimotor, and other), lobes, and gyral subareas.

Results: External globus pallidus segregated into a ventral associative cluster, a dorsal sensorimotor

cluster, and a caudal "other" cluster on the base of its cortical connectivity. Dento-pallidal connections clustered only in the internal globus pallidus, where also associative and sensorimotor clusters were identified. Lobar parcellation revealed the presence in the external globus pallidus of dissociable clusters for each cortical lobe (frontal, parietal, temporal, and occipital), whereas in internal globus pallidus only frontal and parietal clusters were found out.

Conclusion: We mapped the topographical organization of both internal and external globus pallidus according to cortical and cerebellar connections. These anatomical data could be useful in DBS, radiosurgery and MR-guided focused ultrasound targeting for treating motor and nonmotor symptoms in movement disorders. © 2019 The Authors. *Movement Disorders* published by Wiley Periodicals, Inc. on behalf of International Parkinson and Movement Disorder Society.

Key Words: basal ganglia; diffusion MRI; globus pallidus; movement disorders; topographic brain mapping; tractography

The globus pallidus (GP) is subdivided in two functionally independent segments: the internal (GPi) and external (GPe) GP. The GPi is one of the output nuclei

of basal ganglia circuitry together with the SNr, relaying information coming from the striatum, GPe and STN to the thalamus.¹

This is an open access article under the terms of the Creative Commons Attribution License, which permits use, distribution and reproduction in any medium, provided the original work is properly cited.

***Correspondence to:** Dr. Alberto Cacciola, Department of Biomedical, Dental Sciences and Morphological and Functional Images, University of Messina, Via Consolare Valeria, No. 1, 98125 Messina, Italy; E-mail: alberto.cacciola0@gmail.com; or Prof. Angelo Quartarone, Department of Biomedical, Dental Sciences and Morphological and Functional Images, University of Messina, Via Consolare Valeria, No. 1, 98125 Messina, Italy; E-mail: aquartar65@gmail.com

Relevant conflicts of interest/financial disclosures: Nothing to report.

Full financial disclosures and author roles may be found in the online version of this article.

Received: 23 January 2019; **Revised:** 31 March 2019; **Accepted:** 4 April 2019

Published online 11 May 2019 in Wiley Online Library (wileyonlinelibrary.com). DOI: 10.1002/mds.27712

The GPe receives afferents from the striatum and the STN and sends efferents to the striatum, GPi, STN, and SN, suggesting that after the integration in the GPe, information is sent back to other basal ganglia nuclei.²

The classical view of basal ganglia functional anatomy postulates that cortico-basal ganglia-thalamo-cortical pathways are organized in parallel, functionally segregated circuits. This feature allows for the identification of functionally different territories within each nucleus, according to the topographical arrangement of its connections.³

Tracing studies in nonhuman primates revealed that such topographical organization is maintained in the striatum, GP, STN, and SNr.⁴ In particular, polysynaptic pathways linking motor and associative areas to both the GPi and GPe have been described.⁵⁻⁸ When the viruses were injected in the frontal motor areas, neurons were labeled in the dorsal portion of the GPi and GPe,⁷ whereas when viruses were injected in the associative areas, neurons were labeled in the antero-dorsal regions of the GP subdivisions.⁸

Moreover, limbic cortical and subcortical regions are thought to communicate with the antero-ventral part of the GPi through the ventral striatum,^{9,10} whereas connections between limbic areas and GPe are still a matter of debate.¹¹ Taken together, these results suggest the presence of three topographically segregated territories in both the GP divisions: a posterior motor territory, an antero-dorsal associative territory, and an antero-ventral limbic territory.¹¹

Moving from the Nambu's description of a "hyper-direct" cortico-STN pathway,¹² a growing interest to noncanonical connections of the basal ganglia circuitry has arisen. Direct projections from cerebral cortex to both segments of the GP has been already described in different animal species.^{13,14} This scenario has been widely expanded since anatomical studies using retrograde virus tracing demonstrated bidirectional subcortical connections between cerebellum and basal ganglia.^{15,16}

More recently, we used constrained spherical deconvolution (CSD)-based tractography, a diffusion MRI-based technique allowing in vivo reconstruction of connectivity patterns between nervous structures,¹⁷⁻²¹ to study the human analogues of the above-mentioned direct cortico-²² and dento-pallidal projections.²³ These connections, likely paralleled by analogue cortico-²⁴ and dento-nigral^{23,25} pathways, may exert a converging influence of cerebral and neocerebellar cortex on the basal ganglia output nuclei.

Connectivity-based parcellation is a segmentation technique that uses connectivity data to characterize the topographical organization of connections to certain regions of interest (ROIs).^{26,27} This technique, applied to structural probabilistic tractography, has been widely adopted to study the topography of cortico-basal ganglia connections, confirming the organization patterns already described in animals.^{28,29}

This connectivity-based subdivision has recently been extended to the human GPi, in both healthy subjects and Parkinson's disease (PD) carriers.³⁰⁻³² Recently, GPi has been parcellated according to its indirect, thalamo-cortical, and cortico-striatal connectivity.³² To the best of our knowledge, tractography-based parcellation on the GPe has not been carried out yet. Moreover, the mentioned studies evaluated GP topography without discriminating between its indirect (canonical) or direct (non-canonical) pathways.

Herein, aiming at investigating the topographical organization of direct cortico- and dento-pallidal projections on both GP segments, we performed a connectivity-based parcellation of the GPi and GPe on 100 healthy subjects of the Human Connectome Project (HCP) repository.³³

We believe that understanding the topographic organization of cortico- and dento-pallidal connections may (1) shed new light on some neglected anatomical-functional features of the basal ganglia circuitry, (2) improve our knowledge on the pathophysiology of basal ganglia disorders, and (3) improve our understanding of mechanisms underlying DBS, radiosurgery and MR-guided focused ultrasound (FUS) targeting for the treatment of movement disorders.

Materials and Methods

Subjects and Data Acquisition

High-quality structural and diffusion MRI data from the HCP repository have been used. Data were acquired by the Washington University, University of Minnesota, and Oxford University (WU-Minn) HCP Consortium.³³ All HCP subjects were scanned using a Siemens 3T Skyra scanner (Siemens Healthcare, Erlangen, Germany) previously modified with a Siemens SC72 gradient coil and stronger gradient power supply with maximum gradient amplitude of 100 mT/m (initially 70 and 84 mT/m in the pilot phase), with the aim of improving diffusion imaging.³⁴ The HCP database consisted in 100 healthy subjects (males = 46, females = 54; age range: 22–36 years). Structural scans included T₁-weighted images with the following parameters: echo time = 2.14 ms, repetition time = 2,400 ms, and voxel size = 0.7 mm.³⁵ Diffusion-weighted images were acquired using a single-shot two-dimensional (2D) spin-echo multiband echo planar imaging (EPI) sequence and equally distributed over three shells (*b* values of 1,000, 2,000, and 3,000 s/mm²), with isotropic spatial resolution of 1.25 mm.³⁶

Data preprocessing, namely correction of EPI susceptibility, eddy-current-induced distortions, gradient nonlinearities, and subject motion, as well as within-subject co-registration of structural and diffusion images, were already carried out on the downloaded data.³⁷

MRI Images Postprocessing

Both structural and diffusion images were post-processed in order to perform tractography. For each subject, structural images underwent brain extraction³⁸ and cortical and subcortical segmentation^{39,40} by using BET, FAST, and FIRST FSL tools.⁴¹ The obtained masks were visually inspected and, if needed, manually modified by a trained neuroanatomist. A five-tissue segmentation was then gathered by means of FSL tools and used as a prior to run multishell, multitissue CSD (MSMT-CSD).^{42,43} MSMT-CSD represents a variant to the standard CSD approach, which is designed to support multishell data and to overcome classical CSD limitations in presence of tissue-type heterogeneity.⁴⁴ CSD-based computations and tractography were carried out using MrTrix software, release 3 (www.mrtrix.org).⁴⁵

Probabilistic Tractography

Probabilistic whole-brain tractography was run for each subject by generating 10 million streamlines. Anatomically constrained tractography (ACT) was implemented in this step, allowing for a more effective use of the information available from five-tissue anatomical image segmentation.⁴⁶ Spherical harmonic degree was fixed to 6 to obtain robustness to noise. During tractography, tracking was stopped in one of the following conditions: step size = 0.2 mm, maximum angle = 10 degrees, and minimal fiber orientation density function amplitude = 0.15.

Then, obtained whole-brain tractograms were filtered by using the SIFT (Spherical-deconvolution Informed Filtering of Tractograms) algorithm, in order to exclude streamlines that do not appropriately fit the diffusion data, thus improving the accuracy of the reconstruction.⁴⁷ This procedure resulted in a 1-million-streamlines filtered tractogram that has been finally used for tractography-based segmentation.

ROI Segmentation

ROIs for the GPe and GPi were extracted from the Keuken and Forstmann's 7T Atlas of the Basal Ganglia⁴⁸ and registered to the native space of each subject. Dentate ROI was extracted from the SUIT cerebellar template,⁴⁹ as provided in the SPM toolbox. Finally, cortical ROIs were automatically segmented by using the Desikan-Killiany cortical atlas featured in the Freesurfer software.⁵⁰ Different grouping criteria were used for ROI selection to study the topographical organization of connectivity patterns at different levels. In the first level of analysis, cortical ROIs were merged into function-related groups, in line with previous works^{26,32}; the cortex was divided into a limbic group (including orbitofrontal, frontopolar cortices and the anterior cingulate gyri), an associative group (comprising all the remaining prefrontal cortices), a sensorimotor group (including the pre- and postcentral gyri), and the "other"

group, including the remaining cortical regions. At a second level, ROIs were grouped in brain lobes: four cortical lobar ROIs (frontal, temporal, parietal, and occipital) and the dentate nucleus ROI were obtained for each hemisphere. Each lobar ROI was further subdivided into gyral subregions to study the topographical organization of the connections within each lobar cluster. Frontal subareas consisted of: precentral gyri, paracentral lobule, superior frontal gyri (SFG), middle frontal gyri, and inferior frontal gyri. The parietal lobe was subdivided into postcentral gyri, inferior and superior parietal lobules, medial parietal (retrosplenial and isthmus of cingulate cortex), and supramarginal gyri. Temporal areas consisted of transverse temporal gyri, superior, middle, and temporal gyri, and fusiform gyri. Occipital areas included pericalcarine area, lateral occipital area, and lingual gyri.

Connectivity-Based Parcellation

Connectivity-based parcellation was performed using the following pipeline. First, tracts between GPi, GPe, and the selected ROIs were extracted from the filtered 1-million-streamlines whole-brain tractogram described above. Then, each tractogram was converted into a track-density image (TDI), that is, an image where intensity is defined as the number of fiber tracts passing through a given grid element (in this case, a voxel dimensionally equivalent to those of the chosen ROI).⁵¹ Endpoints of tractogram TDI images were then mapped on the GPi and GPe ROIs by multiplying each tractogram image for the corresponding binarized ROI mask, retrieving connectivity density-weighted clusters. Each cluster has been normalized by dividing voxel intensities by the mean intensity within the whole cluster, thus obtaining comparable values across subjects. Finally, a hard segmentation strategy was applied to attribute a voxel exclusively to a selected cluster according to its connectivity strength compared to the others ("winner takes all" method).²⁶ The output consisted in maps of GPe and GPi in which each voxel is attributed to the cluster showing highest connectivity strength. Those maps were then warped, for each subject, to the MNI152 space, binarized and summed up to realize an average parcellation cluster. A 50% threshold was applied to the resulting maps: that is, only voxels overlapping in at least 50 of 100 subjects were considered as being part of the final connectivity-based cluster.

Volumes and Centers of Gravity (CoG) in the Montreal Neurological Institute (MNI) space were extracted from each cluster obtained at a 50% threshold.

Connectivity Analysis

Quantitative connectivity was evaluated using a streamline density index (SDI),⁵² computed as the

percentage ratio between cluster volume and the whole GP volume:

$$SDI = \frac{v}{V_{ROI}} \times 100$$

in which *v* is the volume (expressed in voxels) of each cluster and *V_{ROI}* is the volume (in voxels) of GP.

In addition, the lateralization index (LI)⁵³ was calculated on volumes of topographical maps in subject space and SDI:

$$LI = \frac{Left - Right}{Left + Right}$$

Positive values of LI indicate left lateralization (LI > 0.1), whereas negative values indicate right lateralization (LI < 0.1). For each pathway, in order to assess statistically significant lateralization, permutation tests based on a t-statistic were performed using the connectivity profiles of each hemisphere gathered from each subject. Fifty thousand permutations were used to estimate distribution of the null hypothesis, alpha level was set to 0.05, and the “t-max” method was adopted to correct the *P* values of each variable for multiple comparisons.⁵⁴ LI analysis was performed by means of MATLAB software package (release 2016; www.mathworks.com).

Results

Parcellation clusters derived by our hypothesis-driven parcellation are described below. SDI values are reported for each cluster (mean ± standard deviation). Volumes and CoG of each cluster are summarized in Tables 1–3.

Average parcellation clusters at functional and lobar levels are reported in Supporting Information Figures S1 to S4 for functional territories and Supporting Information Figures S5 to S9 for lobar subdivisions. The effect of different thresholds (10%, 25%, 35%, 50%, and 75%) on connectivity cluster selection, extension, and organization is discussed in Supporting Information Results and summarized in Supporting Information Figures S10 to S12.

Functional Level

External GP

Territories that clustered in the GPe are represented in Figure 1. Three of the four selected clusters (associative, sensorimotor, and “other”) consistently overlapped among subjects, whereas the connectivity of the limbic regions did not reach a sufficient overlap degree (<50% of subjects in every voxel). The antero-dorsal aspect of GPe was occupied by the associative territory (left = 18.83 ± 4.53%; right = 18.27 ± 4.53%); the posterior dorsal region corresponds to the sensorimotor cluster (left = 13.47 ± 3.28%; right 12.31 ± 4.68%); and the caudal pole includes connections with the other cluster (left = 9.26 ± 2.64%; right = 8.70 ± 3.34%).

Internal GP

Only the associative (left = 4.10 ± 2.63%; right = 3.75 ± 2.30%) and sensorimotor (left = 11.03 ± 4.42%; right = 11.21 ± 4.77%) territories consistently overlapped among subjects within the GPi. Figure 1B depicts these two clusters, both located in the caudal part of the nucleus.

TABLE 1. GP clusters at functional level

GP	Target Region	Left (mm ³)	COG (x,y,z)	Right (mm ³)	COG (x,y,z)
GPe	Sensorimotor	161	113.8, 113.5, 74	185	66.2, 116.2, 75.4
	Associative	327	106.8, 124.6, 75.5	284	72.5, 126, 75.8
	Other	106	115.8, 110.4, 69.1	114	63.9, 112.2, 71.2
GPi	Sensorimotor	68	110.5, 114.2, 69.5	67	68.2, 114.9, 70.7
	Associative	60	108.7, 116.2, 71.3	70	70.9, 117.5, 72.1

The table shows volumes (in mm³) and CoG (in MNI152 space) of the connectivity clusters of GPe and GPi (obtained at the 50% threshold) when cortical areas are grouped into functional territories.

TABLE 2. GP clusters at lobar level

GP	Target Region	Left (mm ³)	COG (x,y,z)	Right (mm ³)	COG (x,y,z)
GPe	Frontal	459	107.6, 123, 75.1	401	71.7, 124.4, 75.6
	Parietal	154	115.1, 111.6, 71.3	179	64.7, 113.7, 73.1
	Temporal	60	115.6, 111.2, 67.3	47	63.1, 110.8, 68.4
	Occipital	87	111.5, 117, 67.6	108	66.3, 115.6, 71.2
GPi	Frontal	122	108.6, 111.4, 70.2	106	70.2, 116.9, 71.4
	Parietal	104	109, 116, 69.2	49	67.7, 114.4, 70.6
	Dentate	205	106.8, 118.9, 68.9	136	73.3, 120.2, 69.6

The table shows volumes (in mm³) and CoG (in MNI152 space) of connectivity clusters (obtained at the 50% threshold) at the lobar level.

TABLE 3. GP clusters at subareas level

GP	Target Region	Left (mm ³)	COG (x,y,z)	Right (mm ³)	COG (x, y, z)	
GPe	Paracentral	78	114.6, 111.3, 73.1	79	65, 113.5, 74.4	
	Precentral	172	113.9, 113.3, 73.6	147	66.3, 116.2, 75.5	
	Superior frontal	194	108, 122.6, 76.5	199	71.8, 124.6, 76.5	
	Middle frontal	234	106.2, 125.1, 75.7	188	72.6, 125.7, 76.1	
	Inferior frontal	171	104.8, 127, 74.4	129	74.3, 128.6, 74.9	
	Inferior parietal	124	115.8, 110.2, 69.9	118	65.2, 114.1, 72.6	
	Superior parietal	73	114.9, 111.8, 70.7	111	64.3, 112.8, 71.9	
	Medial parietal	75	115.4, 110.3, 69.9	130	66.3, 115.4, 73.6	
	Supramarginal	75	115.7, 110.1, 70.3	73	63.8, 111.7, 72.1	
	Postcentral	119	114.3, 112.5, 73.4	104	114.3, 112.5, 73.4	
	GPi	Precentral	64	110.6, 114.1, 69.6	67	68.4, 115.1, 70.8
		Postcentral	46	111.3, 113, 69.7	45	67.6, 114.2, 70.7
Superior frontal		57	106.8, 118.9, 68.9	67	73.3, 120.2, 69.6	

The table shows volumes (mm³) and CoG (in MNI152 space) of connectivity clusters (obtained at the 50% threshold) at the subareas level. [Correction added on May 14, 2019, after first online publication: "lobar level" was changed to "subareas level" in Table 3 caption.]

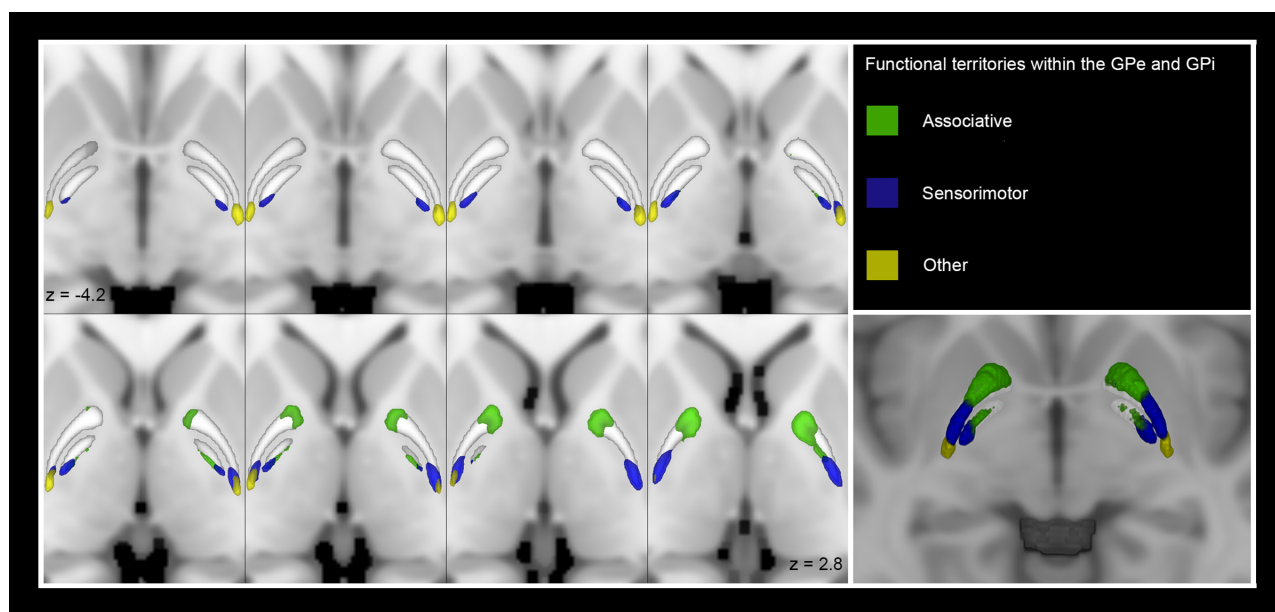


FIG. 1. Multiple axial sections showing the GPe and GPi connectivity clusters (obtained at the 50% threshold) according to functional territories on the MNI template. The clusters have been labeled as follows: sensorimotor (blue), associative (green), and "other" (yellow). On the bottom right corner, a 3D axial section showing functional clusters within the GPe and GPi.

Lobar Level

External GP

Figure 2 shows both 2D slices in the axial plane and a three-dimensional (3D) rendering of the average lobar parcels clustering in the GPe: occipital, temporal, parietal, and frontal lobe clusters. Dentate nucleus did not reach the necessary level of overlap across subjects (<50% of subjects in every voxel). The frontal cluster (left = 28.84 ± 5.47%; right = 26.71 ± 6.36%) occupied a wide portion of the GPe, extending over its antero-dorsal part. The parietal cluster (left = 12.88 ± 3.33%; right 12.18 ± 4.50%) follows posteriorly on the dorsal aspect of the nucleus, whereas the temporal (left = 2.47 ± 1.38%; right = 2.15 ± 1.32%) and occipital (left = 2.24 ± 1.12%; right = 1.03 ± 1.72%) clusters are smaller and confined to the caudal pole

of the GPe. Significant left lateralization was observed for the occipital cluster of GPe both in terms of TDI (LI = 0.372; *P* < 0.01) and SDI (LI = 0.372; *P* < 0.01).

Internal GP

Figure 2 shows both 2D slices in the axial plane and a 3D rendering of the averaged clusters within the GPi: the dentate nucleus and the frontal and parietal lobes. The temporal and occipital lobes did not overlap in more than 50 subjects. The dentate cluster (left = 7.74 ± 5.14%; right = 6.97 ± 4.63%) locates in the anterior-ventral portion of the GPi, whereas the frontal cluster (left = 14.25 ± 5.70%; right = 14.10 ± 5.06%) extends behind it in a more dorsal position; finally, the parietal

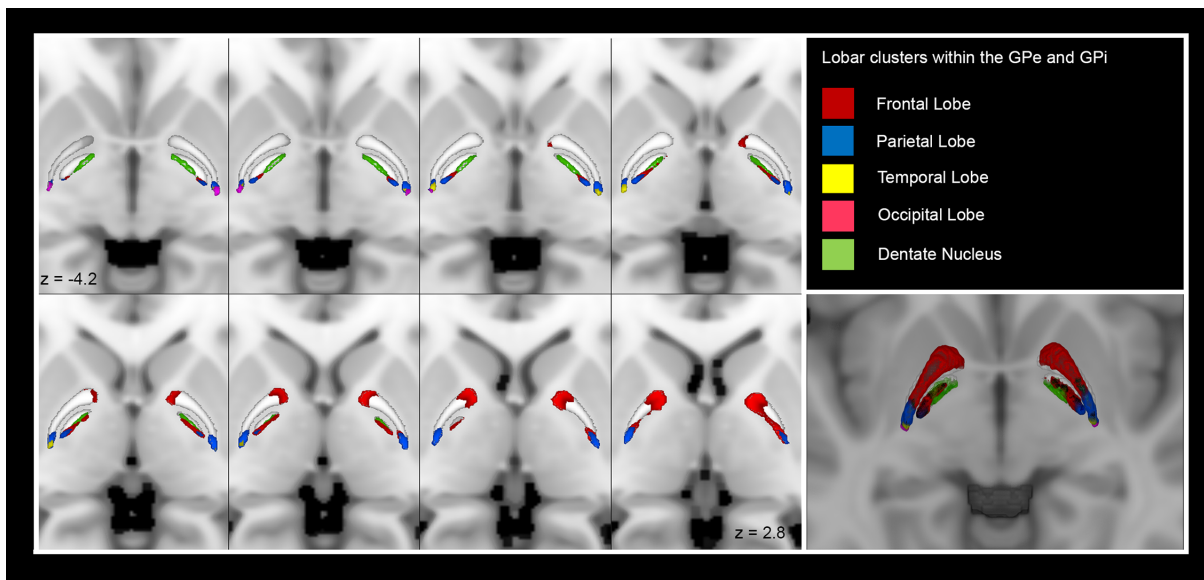


FIG. 2. Multiple axial sections showing the GPe and GPI connectivity clusters (obtained at the 50% threshold) according to lobar cortical targets on the MNI template. The parcels have been labeled as follows: frontal lobe (red), parietal lobe (blue), temporal lobe (yellow), occipital lobe (pink), and dentate nucleus (green). On the bottom right corner, a 3D axial section showing lobar clusters within the GPe and GPI.

cluster (left = $6.36 \pm 3.42\%$; right = $7.01 \pm 3.92\%$) is in the caudal pole of the GPI.

Subareas Level

At the subareas level, each lobar cortical target has been further subdivided in cortical subregions. 3D renderings of subareas clusters are available as Supporting Information (see Supporting Information Figs. S13–S15).

External GP

All the frontal subregions clustered within the dorsal GPe following an antero-posterior topographic pattern: The inferior (left = $6.44 \pm 2.79\%$; right = $5.15 \pm 2.33\%$), middle (left = $9.67 \pm 3.17\%$; right = $7.80 \pm 2.90\%$), and superior (left = $14.53 \pm 3.35\%$; right = $14.80 \pm 3.94\%$) frontal gyri occupied the most anterior part, followed by the large precentral (left = $11.57 \pm 3.00\%$; right = $10.21 \pm 4.00\%$) cluster and the smaller caudal paracentral (left = $2.31 \pm 1.37\%$; right = $2.46 \pm 1.41\%$) cluster. Clusters of parietal subareas follow the same postero-anterior orientation: inferior parietal lobule (left = $2.78 \pm 1.22\%$; right = $2.68 \pm 1.29\%$); medial parietal areas (left = $2.10 \pm 1.29\%$; right = $2.38 \pm 1.40\%$); supramarginal gyrus (left = $3.39 \pm 1.50\%$; right = $2.32 \pm 1.57\%$); postcentral gyrus (left = $7.76 \pm 2.36\%$; right = $6.28 \pm 3.03\%$); and superior parietal lobule (left = $6.08 \pm 1.96\%$; right = $4.99 \pm 2.40\%$). When looking at occipital and temporal subareas, only the lateral occipital cortex and the transverse temporal gyrus clustered respectively.

Internal GP [Correction added on May 14, 2019, after first online publication: Results subheading “Internal Globus Pallidus” was changed to “Internal GP”.]

The postcentral gyrus (left = $3.74 \pm 2.15\%$; right = $4.60 \pm 2.60\%$) and precentral gyrus (left = $9.98 \pm 4.08\%$; right = $9.98 \pm 4.02\%$) resulted to cluster in the most caudal portion, whereas the SFG (left = $4.38 \pm 2.68\%$; right = $4.37 \pm 2.32\%$) clustered in the anterior aspect, ventrally to the dentate nucleus cluster.

Discussion

The purpose of this study was mapping in vivo the topographical organization of the cortico- and dento-pallidal pathways within the GPI and GPe by means of MRI based tractography.

Our findings revealed remarkable differences between the connectivity patterns of GPI and GPe. If, on the one hand, it seems that the cortico-GPe connections are more represented than the cortico-GPI ones, on the other hand, our data suggest that dento-pallidal connections are more represented in GPI than in GPe, where it was not possible to robustly identify a defined connectivity cluster for dento-pallidal connections in any of the thresholds explored, but at the 10% (Supporting Information Fig. S10).

As a fundamental premise, it is worthwhile mentioning that our work suffers from the intrinsic limitations of tractography: its dimensional scale does not allow the visualization of axons, and it is not able to detect the direction of connections and presence of synapses.⁵⁵ To

partially overcome these limitations, we utilized ACT and SIFT algorithms in order to enhance biological accuracy of streamlines tractography deleting potentially spurious tracts which do not fit the deconvolution signal.⁴⁷

Connectivity-based parcellation yields connectivity maps that can be interpreted merely as spatial hypotheses on structural segregation of brain structures.²⁷ Our results should then be interpreted as possible evidences of the structural topography of GP based on cortical and dentate connections, and multimodal data coming from microdissection, cyto-, myelo-, and receptor-architectonics, functional neuroimaging, and other morphofunctional techniques would help in corroborating these hypotheses.

In addition, hypothesis-driven, connectivity-based parcellation may introduce a selection bias.²⁶ The choice of a winner-takes-all parcellation model can introduce a bias by showing only the highest connected voxels and thus by imposing a stricter parcellation in respect to anatomical reality.

Moreover, the choice of an intensity threshold to define a connectivity cluster still represents a matter of debate given that, to the best of our knowledge, no gold-standard methods exist to define a proper threshold; thus, this choice remains rather empirical. In the present work, we used a threshold of 50%, that is, only voxels overlapping in at least 50 over 100 subjects were taken into account. This threshold has been extensively used in recent studies^{30,56} and represents a rather conservative threshold, in comparison with those used in other works.^{31,57} Moreover, to prove that threshold selection does not alter structural connectivity-based topography of the human GP, we explored a range of different thresholds (10%, 25%, 35%, 50%, and 75%), showing that the overall topographic organization of both GPi and GPe is substantially preserved across all thresholds.

However, given that our hypothesis is based on anatomical past knowledge, we believe that a hypothesis-driven approach better fits our study design. Nonetheless, the application of other connectivity parcellation methods would be beneficial to confirm and empower our results.

In humans, topographical organization of the GP results in an antero-ventral limbic region, an antero-dorsal associative region, and a posterior sensorimotor region, both for cortico-striato-pallidal and pallido-thalamic connections.^{28,32,58,59} In line with these findings, we observed a similar organization for the cortico-pallidal pathway. Surprisingly, a well-defined limbic territory was not clearly identified, neither in the GPe nor in the GPi. This might suggest that the direct cortico-pallidal pathway provides a limited contribution to limbic territories of the GP. Noteworthy, the most anterior region of the GP, that should correspond to the limbic territory, is not occupied by any cluster deriving neither from

cortico-pallidal nor from dentate-pallidal connectivity. More details about this topographical organization are given from the examination at the lobar and subareas connectivity-based parcellation levels.

The GPe has been described as a crucial structure for the processing of motor information to the basal ganglia.⁶⁰ Electrophysiological studies on GPe neurons showed a correlation between firing patterns and cinematic properties of movement.⁶¹⁻⁶⁴ Changes in the firing pattern have been demonstrated occurring in a context-related way, thus suggesting an integrative process between movement and sensory information.⁶⁴

Apart from pure motor function, the GPe is thought to integrate motor, cognitive, and reward-related information.⁶⁵ Recorded activity from GPe neurons in specific subregions revealed that activity of each different compartment is strongly influenced from the others: Few neurons of the GPe discharged encoding exclusively motor parameters, whereas most of them encoded both for motor parameters, force required (cognitive) and expected reward (limbic).⁶⁶⁻⁶⁸ Nougaret and Ravel hypothesized that such convergence is highly suggestive of a role of the GPe in updating consequences of actions on motivational information.⁶⁶ In this regard, our results from subareas analysis point out that sensorimotor information may reach the GPe from the postcentral gyrus, precentral gyrus, and paracentral lobule.

On the other hand, the GPi is a key output nucleus of the basal ganglia mainly involved in, but not limited to, somato-motor behaviors. According with this view, the GPi seems to be more connected with sensorimotor cortical areas, as revealed by its functional and lobar parcellation clusters.

A similar arrangement has been observed by Draganski and colleagues, who showed that sensorimotor areas clustered posteriorly to areas belonging to the dorso-lateral prefrontal cortex following a rostro-caudal gradient.²⁹ Even if the aforementioned study did not consider direct cortico-pallidal projections, more recently, the sensorimotor domain of GPi has been parcellated on PD patients. According to this study, the sensorimotor cluster consisted of motor and premotor areas; in particular, M1 clustered posteriorly in respect to prefrontal cortex, in line with our results.³¹ The most represented connectivity patterns to GPi derive from sensorimotor areas and the cerebellum; therefore, it is tempting to speculate a prominent role of a possible cortico-pallidal-cerebellar connectivity in sensorimotor integration.

The presence of a direct cerebello-pallidal pathway is apparently in contrast with findings in primates showing the existence of a topographically organized di- or trisynaptic projection from both motor and nonmotor domains of the dentate nucleus, passing through the thalamus and reaching the putamen or the external segment of the globus pallidus.⁶⁹ Hence, current results should be interpreted with a grain of salt and caution,

also taking into account the well-known limits of tractography in distinguishing between direct or indirect connections⁵⁵ and the current lack of detailed anatomical ground truth on these projections in animal models or in human anatomical postmortem dissections.

Nevertheless, our results, in line with previous investigations,^{23,25,70} may suggest the possible existence of a direct dento-pallidal connection in the human brain. Although highly speculative, it can be hypothesized that a direct dento-pallidal route may represent a fast conducting system that appeared phylogenetically later, in humans, triggered by the emergent importance of manual dexterity.⁷¹

This integrated cortico-pallidal-cerebellar loop would provide the physiological background for flexible motor behavior through a fast upstream control of direct and indirect pathway.

Pathophysiological Implications in Movement Disorders

Interest on the cortico-pallidal route is rapidly spreading. In our previous study, direct cortico-pallidal connections were reconstructed, for the first time, by means of CSD-based tractography.^{13,14,22,72} This hypothesis has been further confirmed by the identification of glutamatergic vesicular glutamate transporter 1 cortical terminals which are widely represented along the GPe and less expressed in the GPi, which is supposed to receive cortical connections to a lesser extent.⁷²

There are other indirect evidences suggesting the presence of cortico-pallidal connections. A combined local field potential recording/magnetoencephalography study in dystonic patients implanted with DBS electrodes revealed three distinct and frequency-specific networks: a temporo-pallidal source of theta band coherence, a cortico-pallidal source of beta band coherence, and a pallido-cerebellar source of alpha band coherence. Interestingly, this latter network was inversely correlated with symptom severity of dystonia.⁷³ Moreover, a recent study conducted on implanted patients with primary cervical dystonia showed a short latency facilitatory effect at 6 ms between GPi and motor cortex, suggesting a rapid and likely direct cortico-pallidal interplay.⁷⁴ Taken together, these results may be indicative of a possible clinical role for cortico- and dento-pallidal connections in the pathophysiology of movement disorders. Future studies are needed to unravel structural plasticity within cortico-basal ganglia networks from the early stages of PD, dystonia, and other movement disorders to better understand adaptive versus maladaptive changes.

Recently, DBS has arisen to the forefront as a highly effective, safe, and useful therapy for movement disorders, especially for dystonia, but also for PD.⁷⁵ In particular, GPi stimulation in parkinsonian patients has been proven to provide fairly equivalent improvement

compared to STN stimulation in treating motor symptoms, while being less affected by the cognitive and behavioral side effects typically described after STN implanting.⁷⁶

On the other hand, DBS of the GPe, although not currently used in clinical practice, has been indicated as a potential target for treatment given that it reduces discharge rate and bursting in GPi and STN in MPTP-treated monkeys.⁷⁷ Moreover, a PET study on patients with Huntington's disease revealed that bilateral GPe-DBS modulated connectivity within the basal ganglia/thalamocortical circuits and sensorimotor and default mode networks, promoting integration across these networks and therefore suggesting its potential role as a therapeutic target.⁷⁸⁻⁸⁰

In this framework, segmentation of the GP, based on multimodal structural and functional imaging in the setting of DBS, could improve patient outcome minimizing side effects. For example, Middlebrooks and colleagues showed that when a DBS electrode is located within the GP sensorimotor territory, the increase of volume tissue activated in the sensorimotor territory is correlated with improvement in the UPDRS.³¹

Our multilevel pallidal parcellation, conducted on 100 healthy subjects, may allow a better understanding on why stimulation of different functional territories in GP leads to variable clinical outcomes. ■

Acknowledgments: Data were provided by the Human Connectome Project, WU-Minn Consortium (Principal Investigators: David Van Essen and Kamil Ugurbil; 1U54MH091657), funded by the 16 NIH institutes and centers that support the NIH Blueprint for Neuroscience Research; and by the McDonnell Center for Systems Neuroscience at Washington University.

References

1. Nambu A. Globus pallidus internal segment. *Prog Brain Res* 2007; 160:135-150.
2. Kita H. Globus pallidus external segment. *Prog Brain Res* 2007;160: 111-133.
3. Alexander G. Parallel organization of functionally segregated circuits linking basal ganglia and cortex. *Annu Rev Neurosci* 1986;9: 357-381.
4. Nambu A. Somatotopic organization of the primate basal ganglia. *Front Neuroanat* 2011;5:1-9.
5. Hoover JE, Strick PL. The organization of cerebellar and basal ganglia outputs to primary motor cortex as revealed by retrograde transneuronal transport of herpes simplex virus type 1. *J Neurosci* 1999; 19:1446-1463.
6. Kelly RM, Strick PL. Rabies as a transneuronal tracer of circuits in the central nervous system. *J Neurosci Methods* 2000;103:63-71.
7. Akkal D, Dum RP, Strick PL. Supplementary motor area and presupplementary motor area: targets of basal ganglia and cerebellar output. *J Neurosci* 2007;27:10659-10673.
8. Ishida H, Inoue K, Takada M, Hoshi E. Origins of multisynaptic projections from the basal ganglia to the forelimb region of the ventral premotor cortex in macaque monkeys. *Eur J Neurosci* 2016;43:258-269.

9. Spooen WPJM, Lynd-Balta E, Mitchell S, Haber SN. Ventral pallidostriatal pathway in the monkey: evidence for modulation of basal ganglia circuits. *J Comp Neurol* 1996;370:295–312.
10. François C, Grabli D, McCairn K, et al. Behavioural disorders induced by external globus pallidus dysfunction in primates II. Anatomical study. *Brain* 2004;127:2055–2070.
11. Saga Y, Hoshi E, Tremblay L. Roles of multiple globus pallidus territories of monkeys and humans in motivation, cognition and action: an anatomical, physiological and pathophysiological review. *Front Neuroanat* 2017;11:1–12.
12. Nambu A, Tokuno H, Takada M. Functional significance of the cortico-subthalamo-pallidal “hyperdirect” pathway. *Neurosci Res* 2002;43:111–117.
13. Naito A, Kita H. The cortico-pallidal projection in the rat: an anterograde tracing study with biotinylated dextran amine. *Brain Res* 1994;653:251–257.
14. Leichnetz GR, Astruc J. The course of some prefrontal corticofugals to the pallidum, substantia innominata, and amygdaloid complex in monkeys. *Exp Neurol* 1977;54:104–109.
15. Bostan AC, Dum RP, Strick PL. The basal ganglia communicate with the cerebellum. *Proc Natl Acad Sci U S A* 2010;107:8452–8456.
16. Bostan AC, Dum RP, Strick PL. Cerebellar networks with the cerebral cortex and basal ganglia. *Trends Cogn Sci* 2013;17:241–254.
17. Milardi D, Cacciola A, Cutroneo G, et al. Red nucleus connectivity as revealed by constrained spherical deconvolution tractography. *Neurosci Lett* 2016;626:68–73.
18. Milardi D, Cacciola A, Calamuneri A, et al. The olfactory system revealed: non-invasive mapping by using constrained spherical deconvolution tractography in healthy humans. *Front Neuroanat* 2017;11:1–11.
19. Cacciola A, Calabrò RS, Costa A, Naro A, Milardi D, Bruschetta D. Enlarged Virchow-Robin spaces in a young man: a constrained spherical deconvolution tractography study. *Acta Biomed* 2017;88:319–324.
20. Cacciola A, Milardi D, Calamuneri A, et al. Constrained spherical deconvolution tractography reveals cerebello-mammillary connections in humans. *Cerebellum* 2017;16:483–495.
21. Rizzo G, Milardi D, Bertino S, et al. The limbic and sensorimotor pathways of the human amygdala: a structural connectivity study. *Neuroscience* 2018;385:166–180.
22. Milardi D, Gaeta M, Marino S, et al. Basal ganglia network by constrained spherical deconvolution: a possible cortico-pallidal pathway? *Mov Disord* 2015;30:342–349.
23. Milardi D, Arrigo A, Anastasi G, et al. Extensive direct subcortical cerebellum-basal ganglia connections in human brain as revealed by constrained spherical deconvolution tractography. *Front Neuroanat* 2016;10:29.
24. Cacciola A, Milardi D, Anastasi GP, et al. A direct cortico-nigral pathway as revealed by constrained spherical deconvolution tractography in humans. *Front Hum Neurosci* 2016;10:374.
25. Cacciola A, Calamuneri A, Milardi D, et al. A connectomic analysis of the human basal ganglia network. *Front Neuroanat* 2017;11:85.
26. Behrens TE, Woolrich MW, Smith SM, et al. Non-invasive mapping of connections between human thalamus and cortex using DTI. *Nat Neurosci* 2003;6:750–757.
27. Eickhoff SB, Thirion B, Varoquaux G, Bzdok D. Connectivity-based parcellation: critique and implications. *Hum Brain Mapp* 2015;36:4771–4792.
28. Lehericy S, Ducros M, Van De Moortele PF, et al. Diffusion tensor fiber tracking shows distinct corticostriatal circuits in humans. *Ann Neurol* 2004;55:522–529.
29. Draganski B, Kherif F, Kloppel S, et al. Evidence for segregated and integrative connectivity patterns in the human basal ganglia. *J Neurosci* 2008;28:7143–7152.
30. da Silva NM, Ahmadi SA, Tafula SN, et al. A diffusion-based connectivity map of the GPi for optimised stereotactic targeting in DBS. *Neuroimage* 2017;144:83–91.
31. Middlebrooks EH, Tuna IS, Grewal SS, et al. Segmentation of the globus pallidus internus using probabilistic diffusion tractography for deep brain stimulation targeting in Parkinson disease. *AJNR Am J Neuroradiol* 2018;39:1127–1134.
32. Patriat R, Cooper SE, Duchin Y, et al. Individualized tractography-based parcellation of the globus pallidus pars interna using 7T MRI in movement disorder patients prior to DBS surgery. *Neuroimage* 2018;178:198–209.
33. Van Essen DC, Smith SM, Barch DM, Behrens TEJ, Yacoub E, Ugurbil K. The WU-Minn Human Connectome Project: an overview. *Neuroimage* 2013;80:62–79.
34. Van Essen DC, Ugurbil K, Auerbach E, et al. WU-Minn HCP Consortium. The Human Connectome Project: a data acquisition perspective. *Neuroimage* 2012;62:2222–2231.
35. Ugurbil K, Xu J, Auerbach EJ, et al. Pushing spatial and temporal resolution for functional and diffusion MRI in the Human Connectome Project. *Neuroimage* 2013;80:80–104.
36. Sotiropoulos SN, Jbabdi S, Xu J, et al. Advances in diffusion MRI acquisition and processing in the Human Connectome Project. *Neuroimage* 2013;80:125–143.
37. Glasser MF, Sotiropoulos SN, Wilson JA, et al. The minimal preprocessing pipelines for the Human Connectome Project. *Neuroimage* 2013;80:105–124.
38. Smith SM. Fast robust automated brain extraction. *Hum Brain Mapp* 2002;17:143–155.
39. Patenaude B, Smith SM, Kennedy DN, Jenkinson M. A Bayesian model of shape and appearance for subcortical brain segmentation. *Neuroimage* 2011;56:907–922.
40. Zhang Y, Brady M, Smith S. Segmentation of brain MR images through a hidden Markov random field model and the expectation-maximization algorithm. *IEEE Trans Med Imaging* 2001;20:45–57.
41. Smith SM, Jenkinson M, Woolrich MW, et al. Advances in functional and structural MR image analysis and implementation as FSL. *Neuroimage* 2004;23(Suppl 1):S208–S219.
42. Tournier JD, Yeh CH, Calamante F, Cho KH, Connelly A, Lin CP. Resolving crossing fibres using constrained spherical deconvolution: validation using diffusion-weighted imaging phantom data. *Neuroimage* 2008;42:617–625.
43. Tournier JD, Calamante F, Connelly A. Robust determination of the fibre orientation distribution in diffusion MRI: Non-negativity constrained super-resolved spherical deconvolution. *Neuroimage* 2007;35:1459–1472.
44. Jeurissen B, Tournier JD, Dhollander T, Connelly A, Sijbers J. Multi-tissue constrained spherical deconvolution for improved analysis of multi-shell diffusion MRI data. *Neuroimage* 2014;103:411–426.
45. Tournier JD, Calamante F, Connelly A. MRtrix: diffusion tractography in crossing fiber regions. *Int J Imaging Syst Technol* 2012;22:53–66.
46. Smith RE, Tournier JD, Calamante F, Connelly A. Anatomically-constrained tractography: Improved diffusion MRI streamlines tractography through effective use of anatomical information. *Neuroimage* 2012;62:1924–1938.
47. Smith RE, Tournier JD, Calamante F, Connelly A. SIFT: spherical-deconvolution informed filtering of tractograms. *Neuroimage* 2013;67:298–312.
48. Keuken MC, Forstmann BU. A probabilistic atlas of the basal ganglia using 7 T MRI. *Data Brief* 2015;4:577–582.
49. Diedrichsen J, Balsters JH, Flavell J, Cussans E, Ramnani N. A probabilistic MR atlas of the human cerebellum. *Neuroimage* 2009;46:39–46.
50. Desikan RS, Ségonne F, Fischl B, et al. An automated labeling system for subdividing the human cerebral cortex on MRI scans into gyral based regions of interest. *Neuroimage* 2006;31:968–980.
51. Calamante F, Tournier JD, Smith RE, Connelly A. A generalised framework for super-resolution track-weighted imaging. *Neuroimage* 2012;59:2494–2503.
52. Theisen F, Leda R, Pozorski V, et al. Evaluation of striatonigral connectivity using probabilistic tractography in Parkinson’s disease. *Neuroimage Clin* 2017;16:557–563.

53. Parker GJ, Luzzi S, Alexander DC, Wheeler-Kingshott CA, Ciccarelli O, Lambon Ralph MA. Lateralization of ventral and dorsal auditory-language pathways in the human brain. *Neuroimage* 2005;24:656–666.
54. Blair CR, Karkiski W. An alternative method for significance testing of waveform difference potentials. *Psychophysiology* 1993;30:518–524.
55. Chung HW, Chou MC, Chen CY. Principles and limitations of computational algorithms in clinical diffusion tensor MR tractography. *AJNR Am J Neuroradiol* 2011;32:3–13.
56. Zhang Y, Larcher KM-H, Misisic B, Dagher A. Anatomical and functional organization of the human substantia nigra and its connections. *Elife*. 2017;6:e26653.
57. Middlebrooks EH, Tuna IS, Almeida L, et al. Structural connectivity-based segmentation of the thalamus and prediction of tremor improvement following thalamic deep brain stimulation of the ventral intermediate nucleus. *Neuroimage Clin* 2018;20:1266–1273.
58. Vaillancourt DE, Mayka MA, Thulborn KR, Corcos DM. Subthalamic nucleus and internal globus pallidus scale with the rate of change of force production in humans. *Neuroimage* 2004;23:175–186.
59. Pessiglione M, Schmidt L, Draganski B, et al. How the brain translates money into force: a neuroimaging study of subliminal motivation. *Science* 2007;316:904–906.
60. Hegeman DJ, Hong ES, Hernández VM, Chan CS. The external globus pallidus: progress and perspectives. *Eur J Neurosci* 2016;43:1239–1265.
61. Georgopoulos AP, Schwartz AB, Kettner RE. Neuronal population coding of movement direction. *Science* 1986;233:1416–1419.
62. Mitchell SJ, Richardson RT, Baker FH, DeLong MR. The primate globus pallidus: neuronal activity related to direction of movement. *Exp Brain Res* 1987;68:491–505.
63. Turner RS, Anderson ME. Pallidal discharge related to the kinematics of reaching movements in two dimensions. *J Neurophysiol* 1997;77:1051–1074.
64. Gage GJ, Stoetzner CR, Wiltchko AB, Berke JD. Selective activation of striatal fast-spiking interneurons during choice execution. *Neuron* 2010;67:466–479.
65. Gittis AH, Berke JD, Bevan MD, et al. New roles for the external globus pallidus in basal ganglia circuits and behavior. *J Neurosci* 2014;34:15178–15183.
66. Nougaret S, Ravel S. Dynamic encoding of effort and reward throughout the execution of action by external globus pallidus neurons in monkeys. *J Cogn Neurosci* 2018;30:1130–1144.
67. Parent A, Hazrati L. Functional anatomy of the basal ganglia. *Brain Res Rev* 1995;20:91–127.
68. Arkadir D. Independent coding of movement direction and reward prediction by single pallidal neurons. *J Neurosci* 2004;24:10047–10056.
69. Hoshi E, Tremblay L, Féger J, Carras PL, Strick PL. The cerebellum communicates with the basal ganglia. *Nat Neurosci* 2005;8:1491–1493.
70. Pelzer EA, Hintzen A, Goldau M, von Cramon DY, Timmermann L, Tittgemeyer M. Cerebellar networks with basal ganglia: Feasibility for tracking cerebello-pallidal and subthalamo-cerebellar projections in the human brain. *Eur J Neurosci* 2013;38:3106–3114.
71. Cacciola A, Milardi D, Livrea P, Flace P, Anastasi G, Quartarone A. The known and missing links between the cerebellum, basal ganglia, and cerebral cortex. *Cerebellum* 2017;16:753–755.
72. Smith Y, Wichmann T. The cortico-pallidal projection: an additional route for cortical regulation of the basal ganglia circuitry. *Mov Disord* 2015;30:293–295.
73. Neumann WJ, Jha A, Bock A, et al. Cortico-pallidal oscillatory connectivity in patients with dystonia. *Brain* 2015;138:1894–1906.
74. Ni Z, Hallett M, Chen R. Reply to “Corticopallidal connectivity: Lessons from patients with dystonia.” *Ann Neurol* 2018;84:159.
75. Larson PS. Deep brain stimulation for movement disorders. *Neurotherapeutics* 2014;11:465–474.
76. Follett KA, Weaver FM, Stern M, et al. Pallidal versus subthalamic deep-brain stimulation for Parkinson’s disease. *N Engl J Med* 2010;362:2077–2091.
77. Vitek JL, Zhang J, Hashimoto T, Russo GS, Baker KB. External pallidal stimulation improves parkinsonian motor signs and modulates neuronal activity throughout the basal ganglia thalamic network. *Exp Neurol* 2012;233:581–586.
78. Beste C, Mückschel M, Elben S, et al. Behavioral and neurophysiological evidence for the enhancement of cognitive control under dorsal pallidal deep brain stimulation in Huntington’s disease. *Brain Struct Funct* 2015;220:2441–2448.
79. Wojtecki L, Groiss SJ, Hartmann CJ, et al. Deep brain stimulation in Huntington’s disease—preliminary evidence on pathophysiology, efficacy and safety. *Brain Sci* 2016;6:E38.
80. Ligot N, Krystkowiak P, Simonin C, et al. External globus pallidus stimulation modulates brain connectivity in Huntington’s disease. *J Cereb Blood Flow Metab* 2011;31:41–46.

Supporting Data

Additional Supporting Information may be found in the online version of this article at the publisher’s web-site.